PHYSICAL REVIEW E **80**, 025602(R) (2009)

Wave localization in strongly nonlinear Hertzian chains with mass defect

Stéphane Job,[1] Francisco Santibanez,[2] Franco Tapia,[2] and Francisco Melo[2]
[1]*Supmeca, 3 rue Fernand Hainaut, 93407 Saint-Ouen Cedex, France*
[2]*Departamento de Física and Center for Advanced Interdisciplinary Research in Materials (CIMAT), Universidad de Santiago de Chile, Avenida Ecuador 3493, Casilla 307, Correo 2, Santiago, Chile*
(Received 20 January 2009; revised manuscript received 23 July 2009; published 24 August 2009)

We report observations of mechanical energy localization in a strongly nonlinear discrete lattice. The experimental setup we consider is a one-dimensional nonloaded horizontal chain of identical spheres interacting via the nonlinear Hertz potential which contains a mass defect. Our experiments show that the interaction of a solitary wave with a light intruder excites a nonlinear localized mode. In agreement with dimensional analysis, we find that the frequency of localized oscillations exceeds the incident wave frequency spectrum and nonlinearly depends on incident wave strength and on mass and size of the intruder. The absence of tensile stress between grains allows some gaps to open, which in turn induces a significant enhancement of the amplitude of oscillations. We performed numerical simulations that precisely describe our observations without any adjusting parameters.

DOI: 10.1103/PhysRevE.80.025602 PACS number(s): 46.40.−f, 05.45.−a, 83.80.Fg, 62.50.−p

Linear wave localization has been studied for long in discrete systems [1] or lattices [2,3]. For instance, the presence of isotopes in crystals are known to enhance optical absorption at given frequencies [4]. In turn, the interplay between discreteness and nonlinearity give rise to novel topological dynamics, such as envelope modes [5], breathers [6], or intrinsic localized modes [7]. The underlying mechanism leading to energy localization in nonlinear lattices is general and relevant for a wide variety of applications, from modern engineering problems to solid-state physics (see [5–8] and references therein). In this frame, one-dimensional nonlinear lattices have received attention since the first efforts of Fermi, Pasta, and Ulam in the mid-1950s [8]. Several investigations have tackled the problem of energy localization in nonlinear lattices with impurities, as for instance in Toda chains [9,10]. Remarkably, these lattices have been shown to share common features regarding energy localization on defects, independently of the potential interaction [11].

One-dimensional chains of elastic spheres (Hertz potential interaction) are systems suitable to observe nonlinear phenomena. In nonloaded chains, energy only propagates as fully nonlinear solitary waves [12–15] resulting from the balance between nonlinearity and nonlinear dispersion due to discreteness [13]. Any heterogeneity capable of unbalancing this equilibrium results in breaking the solitary wave symmetry, as shown for instance in tapered chains [16–18] or in stepped chains [12,19], in which solitary waves broaden or split into trains of solitary waves. Solitary wave trains formation in stepped chains involves stress oscillations localized near the interface [19]. Designing impact protection systems takes advantage of these features [20,21]. Effects of disorder on localization has also been investigated earlier in chains of randomly sized spheres [13] and more recently in diatomic chains with randomly oriented cells [22]. When loaded by static compression, Hertzian chains sustain linear acoustic waves and exhibit frequency band gaps [23], which in turn may lead to wave localization. In all these cases, the presence of defects substantially modifies the dynamics of the lattices. The elementary interaction of either lighter or heavier intruders with shock waves has been investigated numerically [24]. When reached by a shock wave, a heavy impurity slowly translates, leading to a large transmitted solitary waves train in the forward direction [24]. A light intruder oscillates and scatters forward and backward weak delayed solitary wave trains [24].

In this Rapid Communication, we investigate experimentally the dynamics of a single light defect in a nonloaded monodisperse chain of elastic spheres. We observe localized oscillations of the impurity while interacting with a solitary wave. We show that the presence of spatial gap between the intruder and nearest neighbors enhances the oscillation amplitude. A multiscale analysis of the equations of motion of particules allows us to predict the frequency of oscillations as a function of wave strength and intruder mass and size. We also perform high-resolution numerical simulations that capture the experimental features.

Beads are 100*C*6 steel roll bearings [25] with density $\rho = 7780$ kg/m^3, the Young's modulus $Y = 203 \pm 4$ GPa, and Poisson ratio $\nu = 0.3$. The chain is made of 20 equal beads (radius $R = 13$ mm) and contains an intruder ($2.5 \leq R_i \leq 10$ mm) in the middle, as shown in Fig. 1. The beads, barely touching one another, are aligned on a horizontal Plexiglas track. A special short track automatically aligns the intruder on the axis of the chain [18]. The chain is ended by a flat, fixed, and heavy piece of steel. A nonlinear compressive wave (see below) is initiated from the impact of a small striker ($R_s = 4$ mm). The pulse is monitored by measuring the load with a piezoelectric transducer (PCB 200B02, sensitivity 11.24 mV/N, and stiffness 1.9 kN/μm) inserted inside a bead cut in two parts. The total mass of the active bead matches the mass of an original bead and the rigidity of the

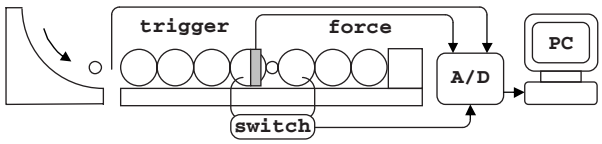

FIG. 1. Experimental setup showing a chain of beads with an intruder, sensors, and acquisition facilities.

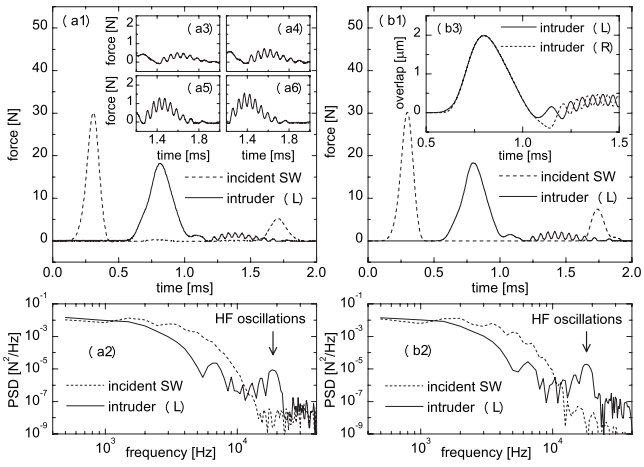

FIG. 2. Panels (a1-a6) are experiments and (b1-b3) are numerical simulations both performed in a monodisperse chain containing a 3 mm in radius intruder. Dashed line in (a1,b1) is the six beads far the intruder incident solitary wave force versus time, and solid line is the force versus time at the left intruder's contact. Power spectral densities of these forces are plotted in (a2,b2), respectively, showing high-frequency content in the intruder force. Closer views of oscillating tail in the intruder's force are shown in (a3-a6) for increasing incident force magnitude (14.1, 17.3, 22.7, and 26.3 N, respectively). Solid and dashed lines in (b3) represent overlaps between the intruder and left and right neighbor beads, respectively.

sensor is comparable to bead's material properties. The embedded sensor thus allows nonintrusive measurements of the force inside the chain [15].

Typical force signals measured by the embedded sensor in contact with the intruder, plotted in Fig. 2(a1), show that well defined oscillations appear in the tail of the incident solitary wave. The tail corresponds to a slight reflection of the incident pulse on the mass defect. Measured oscillations in the tail of the force are displayed in more details in Figs. 2(a3-a6) for increasing amplitudes of the incident solitary wave. Dissipative processes being negligible [15], conservative numerical simulations (see below) shown in Fig. 2(b1) demonstrate satisfactory agreements with experiments, without any adjusting parameter. Calculated overlaps between the intruder and neighbor beads, shown in Fig. 2(b3) [see also the relative displacements in Fig. 4(a)], demonstrate that oscillations in the tail of the force correspond to localized oscillations of the defect. Figures 2(a2) and 2(b2) depict power spectral densities of experimental and calculated forces, respectively, in which the high-frequency component corresponds to the observed oscillations.

Figure 3 presents a longer force acquisition, in which the incident pulse and the pulse reflected by the rigid end are shown. Force signals exhibit features at two different time scales that are separated by filtering low- or high-frequency contents, as shown in Fig. 3(c). Oscillations are only observed when the intruder is loaded by the solitary wave. In Fig. 3(a), intruder oscillations are only visible in the tail of the incident pulse ($0.0 < t < 1.0$ ms). Stronger and relatively faster oscillations can be observed in the reflected pulse ($1.5 < t < 3.0$ ms), both during the main compression and in the tail. Gap openings between the intruder and neighbor

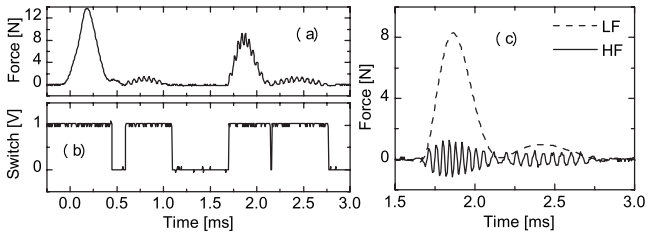

FIG. 3. Force versus time as detected by the embedded sensor in contact with a 3 mm in radius intruder. The first large peak in (a) is the incident solitary wave, and the second one is the wave after being reflected by the rigid end. The gap opening between intruder and nearest beads is indicated in (b) by jumps from upper to lower level in the contact switch. High- and low- frequency components of the force, shown in (c), are obtained by using a tenth order Butterworth filter with zero phase distortion.

beads might explain the differences between incident and reflected pulses features. We designed an electrical switch (smooth metallic brushes in contact with neighbor beads, connected to a fast transistor electrical circuit, see Fig. 1) to detect any loss of contact. The switch is on (1) when beads are in contact and off (0) when loss of contact occurs. As shown in Fig. 3(b), gap first opens right after the incident compression ($t \simeq 0.5$ ms and $t \simeq 2.1$ ms) and second at the end of tail ($t \simeq 1.1$ ms and $t \simeq 2.7$ ms). The first opening is due to the weak reflection of the pulse on the mass defect, and the second one is due to the momentum and energy transfer from the oscillating intruder to neighbors. Higher amplitude oscillations appear provided a gap between the intruder and neighbor exists.

These observations are corroborated by numerical simulation. Indeed, calculated displacements of the intruder and neighbors shown in Fig. 4(a) and the overall gap around the intruder (the difference between left and right neighbor beads displacements) shown in Fig. 4(b) demonstrate that gaps open twice at the intruder, consistently with our experiments. Figure 4(c), showing the intruder displacement relative to the center of mass of the two neighbors beads, reveals that intruder oscillations even exist during the main compression of the incident pulse [$0.5 < t < 1.0$ ms, see magnified view in

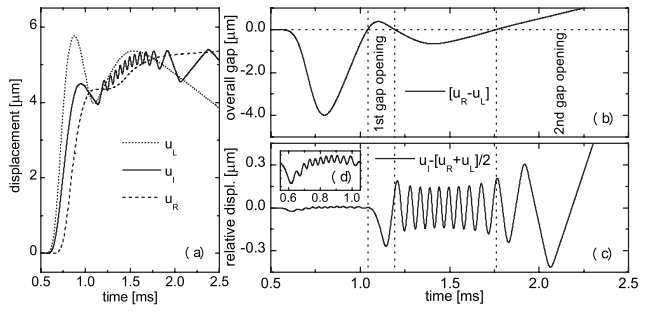

FIG. 4. Numerical simulations of the incident pulse, under same conditions as in Fig. 2(b1). (a) Positions versus time of the intruder and left and right neighbor beads. (b) Overall gap around the intruder demonstrating gap openings occur when a solitary wave crosses the intruder. (c) Intruder displacement relative to the center of mass of the two neighbors beads. (d) Magnified relative displacement during the compression.

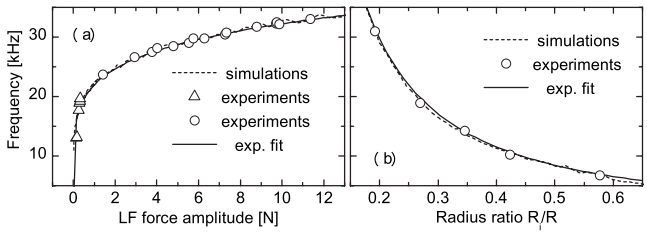

FIG. 5. Panel (a) shows frequency versus force's envelope amplitude for an $R_i=2.5$ mm in radius intruder. Triangles and circles correspond to experimental frequency detected in the tail of the incident pulse and in the reflected pulse, respectively. Panel (b) shows frequency versus intruder's radius measured in the reflected signal, whose envelope amplitude was fixed to $\bar{F}_m=8.7\pm0.6$ N. Dashed lines correspond to numerical simulations and straight lines corresponds to Eq. (4).

Fig. 4(d)]. Momentum transfer is enhanced by larger strain gradient in the presence of gaps.

Next, we analyze how oscillations depend on incident wave strength and on intruder parameters. Frequency of oscillations is obtained from the analysis of power spectral densities of the force. Measurements are repeated nine times and averaged to minimize errors. We first run a set of experiments at constant intruder size ($R_i=2.5$ mm) while varying the amplitude of the incident solitary wave. The force amplitude is obtained from the low-pass filtered signals and results are presented in Fig. 5(a). We then keep the incident pulse amplitude constant (8.7 ± 0.6 N) and test several intruder sizes, as depicted in Fig. 5(b). Experiments show that the frequency of the intruder nonlinearly increases with the incident solitary wave strength and depends on the intruder size.

The physical behavior of solitary waves in chains of equal beads and implications for the existence of localized modes is summarized here. Under elastic deformation, the energy stored at the contact between two elastic bodies submitted to an axial compression corresponds to Hertz potential, $U_H=(2/5)\kappa\delta^{5/2}$, where δ is the overlap deformation between bodies, $\kappa^{-1}=(\theta+\theta')(R^{-1}+R'^{-1})^{1/2}$ and $\theta=3(1-\nu^2)/(4Y)$ are constants, and where R and R' are the respective radii of curvatures at the contact. The force felt at the interface derives from Hertz potential, $F_H=\partial_\delta U_H=\kappa\delta_+^{3/2}$. Index + indicates that Hertz force is zero when the beads loose contact (no tensile force). The dynamics of a chain of beads is thus described by the following system of N-coupled nonlinear equations:

$$m\ddot{u}_n=\kappa[(u_{n-1}-u_n)_+^{3/2}-(u_n-u_{n+1})_+^{3/2}], \tag{1}$$

where m and u_n are the mass and the position of bead n, respectively. Considering long-wavelength perturbations, such that the strain $\psi=(-\partial_x u)\simeq(\delta/2R)\simeq(u/\lambda)\ll1$, a continuous equation can be derived from Eq. (1), which admits an exact solution [13] in the form of a purely compressive and periodic traveling wave, $\psi(x,t)=\psi_m\cos^4[(x-vt)/(R\sqrt{10})]$. Wave speed, $v\propto\psi_m^{1/4}$, nonlinearly depends on maximum strain. Infinitely small perturbations in the acoustic limit propagate at zero speed, linear waves are thus forbidden. One hump of this periodic function represents a solitary wave solution [13]. In addition to analytical estimations, we solve the nonlinear system of Eq. (1) by using a fourth order Runge-Kutta numerical scheme [26], the embedded force sensor being incorporated in simulations for closer comparisons [27]. Numerical time step is few orders of magnitude smaller than the shortest physical duration and energy conservation is fulfilled within a relative error better than 10^{-9}.

The characteristic frequency of localized oscillations can be estimated through a multiscale analysis of Eq. (1). Here, index n denotes the intruder with radius R_i and mass $m_i=(4/3)\pi\rho R_i^3$, and $\kappa_i=\kappa(R,R_i)=\kappa(R_i,R)$ is the elastic constant that depends on radii and properties of the beads. Index $n\pm1$ denote the two neighbor beads with radius $R>R_i$. We consider two distinct time scales: a slow time scale of the order of solitary wave duration and a fast time scale associated with intruder oscillations. Displacements of the intruder and neighbor beads are written as $u_n\simeq\bar{u}_n+\tilde{u}_n e^{i\omega t}$ and $u_{n\pm1}\simeq\bar{u}_{n\pm1}$, where $\bar{u}_n$ and $\tilde{u}_n$ are slowly varying functions of time. Harmonic oscillations amplitude is assumed negligible compared to solitary wave amplitude, $\tilde{u}_n\ll\bar{u}_n$. Using this ansatz into Eq. (1) leads to

$$\ddot{\bar{u}}_n\simeq\frac{\kappa_i}{m_i}[(\bar{u}_{n-1}-\bar{u}_n)_+^{3/2}-(\bar{u}_n-\bar{u}_{n+1})_+^{3/2}], \tag{2}$$

$$\omega^2\simeq\frac{3}{2}\frac{\kappa_i}{m_i}[(\bar{u}_{n-1}-\bar{u}_n)_+^{1/2}+(\bar{u}_n-\bar{u}_{n+1})_+^{1/2}], \tag{3}$$

where the first equation, at leading order, provides the displacement of the intruder at slow time scale. The second equation, at next order, determines the angular frequency of the oscillating intruder. We then introduce slowly varying forces at the contacts of the intruder, $\bar{F}_-=\kappa_i(\bar{u}_{n-1}-\bar{u}_n)_+^{3/2}$ and $\bar{F}_+=\kappa_i(\bar{u}_n-\bar{u}_{n+1})_+^{3/2}$. Noticing that they almost behave in phase [$\bar{F}_+\simeq\bar{F}_-$, see Fig. 2(b3)], the first equation indicates that intruder acceleration oscillates around equilibrium position, $\ddot{\bar{u}}_n\simeq0$. The second equation provides the maximum oscillation frequency $f_m=\max[\omega/2\pi]$ as a function of the amplitude of the slow time force at the intruder contact, $\bar{F}_m\simeq\max[\bar{F}_+]\simeq\max[\bar{F}_-]$:

$$f_m\simeq\frac{3^{1/2}}{2\pi}\frac{\kappa_i^{1/3}\bar{F}_m^{1/6}}{m_i^{1/2}}\simeq C\frac{(R/R_i)^{4/3}\bar{F}_m^{1/6}}{(1+R_i/R)^{1/6}}, \tag{4}$$

where $C=(3/4\pi\sqrt{\pi\rho})/(2\theta R^4)^{1/3}$. Equation (4) shows that oscillation frequency tends to zero when the load vanishes: oscillations stops as soon as the solitary wave leaves the intruder. Using the characteristics of our beads, we find a theoretical estimation, $C_t=2640$ Hz/N$^{1/6}$. Matching Eq. (4) to experiments and simulations shown in Fig. 5, we find $C_e=2510\pm151$ Hz/N$^{1/6}$ and $C_n=2531\pm52$ Hz/N$^{1/6}$, respectively. The agreement among experiments, simulations, and theory shown in Fig. 5 is satisfactory, considering that no adjustable parameters is used between experiments and simulations.

Equation (4) can also be obtained by considering the low-frequency force envelope amplitude, of the order of $\bar{F}_m$, as a

static load at the time scale of fast oscillations, which induces an *in situ* band gap [23]. The dynamics of a loaded monodisperse chain of beads of mass m behaves according to linearized Hertz potential around static equilibrium; the intergrain stiffness reads $k \simeq (3/2)\kappa^{2/3}\bar{F}_m^{1/3}$. Small perturbations propagate as acoustic waves according to the dispersion relation $\omega = (2\sqrt{k/m})|\sin(qR)|$. Forcing a single particle to move at an angular frequency ω above the cutoff $\omega_c = 2\sqrt{k/m}$ generates an evanescent wave since the wave number is $qR = \pi/2 - j\cosh^{-1}(\omega/\omega_c)$. The group velocity $v_g = (\partial \mathrm{Re}[q]/\partial\omega)^{-1}$ is zero and the perturbation remains localized within a characteristic distance $x_c = (\mathrm{Im}[q])^{-1} = R/\cosh^{-1}(\omega/\omega_c)$. Localization achieves when replacing a single particle by a light intruder with mass $m_i \ll m$. Roughly estimating the angular frequency of the intruder from the free oscillation frequency between two heavy nonoscillating neighbors $\omega_i \simeq \sqrt{2k_i/m_i}$, where $k_i \simeq (3/2)\kappa_i^{2/3}\bar{F}_m^{1/3}$, leads to Eq. (4) expression. The frequency of oscillations exceeds the cutoff $\omega_i \gg \omega_c$ and the energy remains localized within a characteristic distance that does not depend on static load and which is smaller than a single radius, $x_c \ll R$.

It should be pointed out that weak delayed solitary wave trains, responsible for nonlinear leak of oscillating energy from the intruder to surrounding [24], were detected few beads before or after the intruder in long duration force acquisitions (not shown in this Rapid Communication). This attenuation mechanism leads to an exponential decay of the oscillating amplitude within a characteristic time much longer than the duration of the low-frequency force envelope, $\tau_{leak}/\tau_{LF} \sim \sqrt{m/m_i} \gg 1$, provided $m_i \ll m$.

In conclusion, we have reported the first experimental observations of energy localization in a strongly nonlinear discrete lattice of elastic spheres. The interaction of a traveling wave with a light defect induces a local strain gradient which excites localized oscillations. The amplitude of these oscillations is enhanced by the presence of spatial gap near the intruder. Localized energy is unable to radiate linear acoustic waves since they are not sustained in adjacent nonloaded chains. Such nonlinear localization traps part of the incident energy and shifts the frequency spectrum according to the incident strength and the mass of the defect; this might play an important role in intense wave mitigation. It is also likely to appear in polydisperse three-dimensional granular assemblies and lead to sound trapping by light weakly loaded grains.

This work was supported by Conicyt under Fondap Research Program No. 11980002.

[1] I. M. Lifshitz, J. Phys. (USSR) **7**, 215 (1943); **7**, 249 (1943); **8**, 89 (1944).
[2] E. W. Montroll *et al.*, Phys. Rev. **100**, 525 (1955).
[3] A. A. Maradudin *et al.*, *Theory of Lattice Dynamics in the Harmonic Approximation*, Solid State Physics, Vol. 3 (Academic Press, New York, 1971).
[4] A. J. Sievers, Phys. Rev. Lett. **13**, 310 (1964).
[5] T. Dauxois and M. Peyrard, Phys. Rev. Lett. **70**, 3935 (1993).
[6] S. Flach and C. R. Willis, Phys. Rep. **295**, 181 (1998).
[7] M. Sato *et al.*, Rev. Mod. Phys. **78**, 137 (2006).
[8] M. Peyrard and T. Dauxois, *Physique des Solitons* (CNRS, Paris, 2004).
[9] S. Watanabe and M. Toda, J. Phys. Soc. Jpn. **50**, 3436 (1981); **50**, 3443 (1981).
[10] Q. Li, S. Pnevmatikos, E. N. Economou, and C. M. Soukoulis, Phys. Rev. B **37**, 3534 (1988).
[11] M. Leo *et al.*, Eur. Phys. J. D **11**, 327 (2000).
[12] V. F. Nesterenko, J. Appl. Mech. Tech. Phys. **24**, 733 (1984); A. N. Lazaridi and V. F. Nesterenko, *ibid.* **26**, 405 (1985).
[13] V. F. Nesterenko, *Dynamics of Heterogeneous Materials* (Springer-Verlag, New York, 2001).
[14] C. Coste, E. Falcon, and S. Fauve, Phys. Rev. E **56**, 6104 (1997).
[15] S. Job, F. Melo, A. Sokolow, and S. Sen, Phys. Rev. Lett. **94**, 178002 (2005).
[16] R. L. Doney and S. Sen, Phys. Rev. E **72**, 041304 (2005).
[17] R. Doney and S. Sen, Phys. Rev. Lett. **97**, 155502 (2006).
[18] F. Melo, S. Job, F. Santibanez, and F. Tapia, Phys. Rev. E **73**, 041305 (2006).
[19] S. Job *et al.*, Granular Matter **10**, 13 (2007).
[20] J. Hong, Phys. Rev. Lett. **94**, 108001 (2005).
[21] C. Daraio, V. F. Nesterenko, E. B. Herbold, and S. Jin, Phys. Rev. Lett. **96**, 058002 (2006).
[22] L. Ponson *et al.*, e-print arXiv:0904.0426.
[23] E. B. Herbold *et al.*, Acta Mech. **205**, 85 (2009).
[24] E. Hascoet *et al.*, Eur. Phys. J. B **14**, 183 (2000).
[25] See, for instance, http://www.marteau-lemarie.fr/
[26] A. Chatterjee, Phys. Rev. E **59**, 5912 (1999).
[27] S. Job *et al.*, Ultrasonics **48**, 506 (2008).